KSME

Springer

Journal of Mechanical Science and Technology 37 (10) 2023

Original Article
DOI 10.1007/s12206-023-0903-x

Keywords:
· Dynamic modeling
· Finite element method
· Maneuvering load
· Rotor-bearing system
· Speed variation

Correspondence to:
Zhang Dahai
dzhang@seu.edu.cn;
Fei Qingguo
qgfei@seu.edu.cn

Citation:
Miao, X., He, J., Zhang, D., Jiang, D., Li, J., Ai, X., Fei, Q. (2023). Nonlinear response analysis of variable speed rotor system under maneuvering flight. Journal of Mechanical Science and Technology 37 (10) (2023) 4957~4971. http://doi.org/10.1007/s12206-023-0903-x

Received February 10th, 2023
Revised May 21st, 2023
Accepted June 29th, 2023

† Recommended by Editor No-cheol Park

Nonlinear response analysis of variable speed rotor system under maneuvering flight

Xueyang Miao[1,2], Junzeng He[1,2], Dahai Zhang[1,2], Dong Jiang[2,3], Jian Li[4], Xing Ai[4] and Qingguo Fei[1,2]

[1]School of Mechanical Engineering, Southeast University, Nanjing 211189, China, [2]Jiangsu Engineering Research Center of Aerospace Machinery, Nanjing 211189, China, [3]School of Mechanical and Electronic Engineering, Nanjing Forestry University, Nanjing 210037, China, [4]China Aviation Power Plant Research Institute, Zhuzhou 412002, China

Abstract Maneuverability is one of the important tactical and technical indexes of fighter aircraft. In this paper, the finite element method is used to establish a dynamic model of the rotor system that can consider arbitrary maneuvering flight form and rotor speed variation during the flight, and the vibration characteristic of the dynamic model is investigated in detail. In addition, the nonlinear forces caused by bearings and oil film are also considered. The Newmark-β method combined with Newton-Raphson method is adopted to solve the dynamic equations. The influences of speed variation, rolling, pitching, and yawing maneuver loads on the vibration responses of the rotor system are also evaluated.

1. Introduction

Maneuverability refers to the flight process in which an aircraft changes its motion state in flight, the greater the overload the aircraft can bear, the better the maneuverability. Therefore, maneuverability is one of the important tactical and technical indicators of the aircrafts, especially the fighters. Modern fighters have high requirements on maneuverability and need to carry out great changes in motion in a short time. However, the rotor of aeroengine is a very complex nonlinear system, and the load caused by maneuvering flight will have a significant effect on the vibration of the rotor system. And during the maneuvering flight, the variable speed rotor can further improve the performance of the aircraft [1].

The rotor system of an aero-engine usually includes bearings, squeeze film damper (SFD) and other structures, which can adjust the vibration and critical speed of the rotor system. Lu et al. [2] took a dual-rotor system considering the influence of bearings as the research object, and analyzed the influence of bearing clearance on rotor vibration characteristics. Based on Euler-Bernoulli beam theory, Amirzadegan et al. [3] established a flexible shaft model on a flexible bearing with springs and a damper, and further analyzed the nonlinear oscillation of the shaft as it passes through the critical speeds. Liu et al. [4] established a dynamic model of the flexible rotor system considering the nonlinear force of the bearing and eccentric force, and analyzed the influence of radial clearance and eccentric on vibration characteristics. Based on the Lagrange equation and Runge-Kutta-Fehlberg method, Li et al. [5] studied the nonlinear dynamic response of the rotor-bearing system with bolted connection structure. Considering the pretightening force, Liu et al. [6] proposed a one-dimensional discrete mass model to improve the rotor modeling efficiency, and verified the accuracy by comparing it with the three-dimensional model. Considering the tangential motion of the rolling element, nonlinear Hertz contact force and internal radial clearance, Wei et al. [7] used the fourth-order Runge-Kutta method to study the nonlinear vibration characteristics of the rotor-bearing-brush seal system, and analyzed the influence of key parameters on the nonlinear vibration. Nan et al. [8] studied the vibration characteristics of rotors with wavy faults by using the variable step-size Runge-

Kutta method, and discussed the effects of waviness, clearance and eccentricity on the vibration characteristics. Jin et al. [9] established the finite element model of the dual-rotor system with different beam elements, and proposed a two-level model order reduction (MOR) to analyze the vibration characteristic of the rotor system. Wang et al. [10] studied the dynamic stiffness of a typical support structure of an aero-engine by combining numerical and experimental methods, and discussed the influence of dynamic stiffness on bearing vibration response. For the first time, Lu et al. [11] used the proper orthogonal decomposition (POD) method to study the dimension reduction of the dual rotor-bearing system, and verified the high computational efficiency and accuracy of the POD method through theoretical and experimental studies. Zhou et al. [12] establish the rotor-bearing model with open cracks and breath cracks, and calculated the stability of the system using the Floquet theory, and discussed the influence of depth and positions of cracks on the stability of the system.

SFD can adjust the vibration and critical speed of the rotor system, but it also brings complex nonlinear behavior. Wang et al. [13] established the rotor system model in the aeroengine, and discussed the suppression ability of SFD on vibration response of the rotor system under different speeds and unbalances. Ma et al. [14] established the finite element model of the dual-rotor system with bearings and SFD, and discussed the influence of bearing parameters, unbalance and oil film parameters on the nonlinear behavior of the rotor system. Wang [15] proposed a floating SFD theoretical model, and used explicit Newmark and implicit Newmark methods to discuss the impact of SFD on the response of the rotor system. Liu et al. [16] established the dynamic model of the turboshaft engine, and studied the nonlinear vibration mechanism of the rotor system considering nonlinear support and rubbing force. Han et al. [17] established the finite element model of the rotor system with the shared support structure and SFD, and discussed the influence of unbalance, radial stiffness, bending stiffness and other factors on the dynamic characteristics of the rotor system. Ri et al. [18] used the incremental harmonic balance (IHB) method and the alternating frequency/time (AFT) method to analyze the nonlinear vibration of a flexible rotor supported on SFDs with centering springs, and investigated the bifurcation phenomena in the resonance region.

In maneuvering flight, additional loads are attached to the rotor system, namely maneuvering load, also known as inertial load or constant excitation. Due to the highly nonlinear characteristics of modern aero-engine, the nonlinear behavior of the rotor will be changed by maneuvering load. Hou et al. conducted many studies on the nonlinear behavior under different loads by using the multi-scale method [19-21]. Using fourth order Runge-Kutta method, Hou et al. [22] considered the pitching maneuver load and studied the vibration response of the rotor-bearing system with cracks. Considering the maneuvering flight, Han et al. [23] established the finite element model of the rotor-ball bearing system, and studied the dynamic characteristics of the rotor system by hybrid numerical method. Gao et al. [24] established a finite element model of the flexible asymmetric rotor system considering bearings and nonlinear supports, and considered the effects of translational acceleration motion, angular motion, and pitching motion on the dynamic characteristics Pan et al. [25] used Newmark-β method to analyze the response of the rotor-bearing system with nonlinear contact force and maneuvering loads, and compared the influence of different maneuvering loads. Nan [26] established the finite element model of the rotor system under arbitrary maneuvering flight conditions, and uses the experimental and theoretical methods to study the vibration characteristics of the rotor system under constant maneuvering load. Pan et al. [27] established a prediction model of the rotor system with rubbing faults, studied the influence of maneuvering load and rub-impact stiffness on the nonlinear dynamics of the system.

As can be seen from the above research that the rotor system will be affected by maneuvering load during flight. At the same time, the speed of the rotor changes with the maneuvering flight of the aircraft to obtain higher performance. These factors will have a great effect on the dynamic behavior of the rotor system, which means that the influence of the maneuvering load and the variation of rotor speed cannot be ignored. Most studies have used simple single-disk rotors, which cannot reflect the complex rotor system characteristics of aero-engines. Therefore, it is necessary to establish a general model which can consider various nonlinear factors to analyze the nonlinear behavior of the rotor system during arbitrary flight maneuvers.

The innovation of this paper is to establish a general dynamic model of the rotor system which can consider arbitrary maneuvering flight form. The more complex and real rotor-bearing system is taken as the research object, and the change of rotor speed is taken into account to simulate the more real working state of the rotor system. Furthermore, the nonlinear Hertz contact force and the nonlinear oil film force were considered, the general dynamic model was established to analyze the dynamic characteristics. And the Newmark-β method combined with Newton-Rapson method was used to analyze the influence of the variation of speed and different maneuvering loads on the vibration characteristics of the rotor system.

2. Mathematical model

As mentioned above, during flight maneuvers, on the one hand, the rotor speed changes, on the other hand, it will be affected by maneuvering load. Therefore, the rotation speed of the rotor system is considered a function of time, and maneuvering loads are divided into different forms according to flight. In this paper, three kinds of maneuvering flight are considered, namely, rolling, pitching and yawing maneuver flight [25]. For the convenience of analysis, the established coordinate system is shown in Fig. 1. The ground coordinate system *O-XYZ* is used to describe the spatial position, velocity and acceleration of the aircraft centroid. The rotor coordinate system *o-xyz* is used to describe the flight of the aircraft, the position and op-

eration status of the rotor system on the aircraft, and the position, velocity, and acceleration of the disk's center of mass on the body.

In this paper, a gas generator rotor in the dual-rotor turboshaft aeroengine is taken as the object of study. The gas generator rotor system is connected to the bearing seat by two supports, and squirrel cage structures and SFDs are considered in the model.

The bearing-rotor system, as the research object, is composed of a central tie rod, a gas turbine, a centrifugal impeller and disks. The rolling bearings are located on both sides of the rotor system. Timoshenko beam element is adopted to establish the finite element model of the rotor system. The lumped mass method is used to express centrifugal disk and disk structures. The disks are simplified as lumped mass points applied to the corresponding nodes, then the displacement of the disk structure is the displacement of the corresponding node. The centrifugal impeller is so large that it is divided into two disks, and they are grouped with the finite element model, then the finite element model can be obtained, as shown in Fig. 2.

2.1 Modeling of maneuvering flight

The loads caused by maneuvering flight will have a great impact on the rotor system. The kinetic energy of the disk in the rotor system under arbitrary maneuvering flight can be divided into translational kinetic energy $\boldsymbol{T}_t$ and rotational kinetic energy $\boldsymbol{T}_r$, in which $\boldsymbol{T}_t$ can be expressed as [26] :

$$\boldsymbol{T}_t = \frac{1}{2} m \begin{pmatrix} \dot{\mathbf{r}}^{\mathrm{T}} \dot{\mathbf{r}} + \mathbf{v}_B^{\mathrm{T}} \mathbf{v}_B - \mathbf{r}^{\mathrm{T}} \bar{\boldsymbol{\omega}}_B^2 \mathbf{r} \\ +2\dot{\mathbf{r}}^{\mathrm{T}} \bar{\boldsymbol{\omega}}_B \mathbf{r} + 2\mathbf{v}_B^{\mathrm{T}} \dot{\mathbf{r}} + 2\mathbf{v}_B^{\mathrm{T}} \bar{\boldsymbol{\omega}}_B \mathbf{r} \end{pmatrix} \tag{1}$$

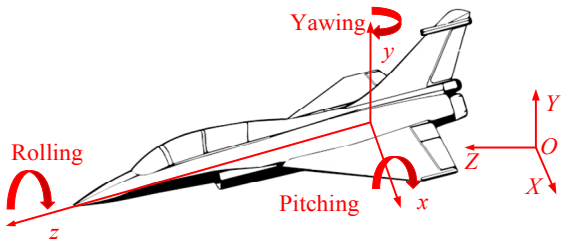

Fig. 1. Schematic diagram of aircraft during flight maneuvers.

where m is the mass of the disk, $\mathbf{r}$ is the relative position of the disk in the coordinate system O-XYZ, $\mathbf{v}_B$ and $\bar{\boldsymbol{\omega}}_B$ are the velocity and angular velocity of the aircraft in the O-XYZ coordinate system, expressed as:

$$\mathbf{r} = \begin{bmatrix} x + e\cos(\omega t + \varphi_0) \\ y + e\sin(\omega t + \varphi_0) \\ z \end{bmatrix}, \mathbf{v}_B = \begin{bmatrix} \dot{X}_B \\ \dot{Y}_B \\ \dot{Z}_B \end{bmatrix},$$
$$\bar{\boldsymbol{\omega}}_B = \begin{bmatrix} 0 & -\omega_z & \omega_y \\ \omega_z & 0 & -\omega_x \\ -\omega_y & \omega_x & 0 \end{bmatrix} \tag{2}$$

where ω is the rotor speed, φ_0 is the initial angle of disk unbalance, $\dot{X}_B$, $\dot{Y}_B$ and $\dot{Z}_B$ are the aircraft velocity along each coordinate axis, ω_x, ω_y, and ω_z are the aircraft angular velocity around each coordinate axis.

The rotational kinetic energy of the disk of the rotor during the maneuvering flight can be expressed as:

$$\begin{aligned} \boldsymbol{T}_r &= \frac{1}{2} J_d \left[\left(\dot{\theta}_y + \omega_y \right)^2 + \left(\dot{\theta}_x + \omega_x \right)^2 \right] \\ &+ \frac{1}{2} J_p \left[\omega^2 + 2\omega \left(\dot{\theta}_y + \omega_y \right) \left(\dot{\theta}_x + \omega_x \right) \right] \end{aligned} \tag{3}$$

where J_d and J_p are the diameter and polar moment of inertia of the disk, and the dissipation and the elastic potential energy of the shaft at the position of the disk can be expressed as

$$\begin{aligned} D &= \frac{1}{2} \dot{q}_d^{\mathrm{T}} C_d \dot{q}_d \\ V &= \frac{1}{2} \dot{q}_d^{\mathrm{T}} K_d \dot{q}_d \end{aligned} \tag{4}$$

where q_d is the degree of freedom of the disks, by substituting equations into Lagrangian equations, the additional damping matrix $\boldsymbol{C}_B$, stiffness matrix $\boldsymbol{K}_B$, and maneuvering load $\boldsymbol{F}_B$ caused by maneuvering flight can be obtained.

The expression of $\boldsymbol{C}_B$ is

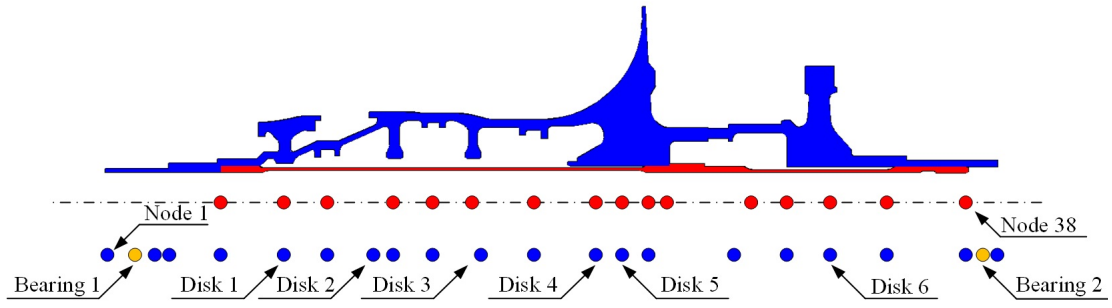

Fig. 2. Schematic diagram of finite element model of rotor-bearing system.

$$\boldsymbol{C}_B=\begin{bmatrix}0 & -2m_i\omega_z & 0 & 0\\ 2m_i\omega_z & 0 & 0 & 0\\ 0 & 0 & 0 & 0\\ 0 & 0 & 0 & 0\end{bmatrix} \tag{5}$$

And the expression for $\boldsymbol{K}_B$ is

$$\boldsymbol{K}_B=\begin{bmatrix}-m_i\left(\omega_y^2+\omega_z^2\right) & m_i\left(\omega_x\omega_y-\omega_z\right) & 0 & 0\\ m_i\left(\omega_x\omega_y+\omega_z\right) & -m_i\left(\omega_x^2+\omega_z^2\right) & 0 & 0\\ 0 & 0 & 0 & 0\\ 0 & 0 & 0 & 0\end{bmatrix} \tag{6}$$

where m_i indicates the mass of the disk and i indicates the number of the disk.

When the aircraft does rolling flight, the expression of $\boldsymbol{F}_B$ is

$$\boldsymbol{F}_B=\begin{bmatrix}0,0,0,0,\cdots 2m_i\omega_z v,0,0,0,\\ \cdots 2m_{sl}\omega_z v_z,0,2m_{sr}\omega_z v,0\end{bmatrix}. \tag{7}$$

When the aircraft does pitching flight, $\boldsymbol{F}_B$ is expressed as:

$$\boldsymbol{F}_B=\begin{bmatrix}0,0,0,0,\cdots\pm m_i\omega_x v,0,\pm J_i\omega\omega_x,0,\\ \cdots\pm m_{sl}\omega_x v,0,\pm m_{sr}\omega_x v_z,0\end{bmatrix} \tag{8}$$

where "+" means that the aircraft is climbing flight, "-" means that the aircraft is diving flight.

When the aircraft does yawing flight, $\boldsymbol{F}_B$ can be expressed as:

$$\boldsymbol{F}_B=\begin{bmatrix}0,0,0,0,\cdots m_i\omega_y v,0,J_i\omega\omega_y,0,\\ \cdots 0,m_{sl}\omega_y v,0,m_{sr}\omega_y v\end{bmatrix} \tag{9}$$

where, ω_x, ω_y, and ω_z are the angular velocities of maneuvering flight of the aircraft, v is the velocity of flight of the aircraft, i is the node position of mass points in the model, m_{sl} and m_{sr} are the masses of left and right SFD.

2.2 Modeling of rotor system

The rotor system contains bearings and SFD, whose mass and stiffness should be attached to the stiffness and mass matrix of the rotor system, expressed as:

$$\begin{aligned}\mathbf{M}_s&=\mathrm{diag}\left[m_{sl}\ \ m_{sl}\ \ m_{sr}\ \ m_{sr}\right]\\ \mathbf{K}_s&=\mathrm{diag}[k_{blx}\ \ k_{bly}\ \ k_{brx}\ \ k_{bry}]\end{aligned} \tag{10}$$

where m_{sl} is the concentrated mass of the inner oil film ring and the outer ring of the rolling bearing on the left SFD, k_{blx} and k_{bly} are the stiffness of the elastic support on the left. m_{sr}, k_{brx}, and k_{bry} are the parameters corresponding to SFD on the right. Then, the mass and stiffness matrix of the rotor system can be expressed as:

$$\boldsymbol{M}=\begin{bmatrix}\boldsymbol{M}_r & \boldsymbol{0}\\ \boldsymbol{0} & \boldsymbol{M}_s\end{bmatrix},\boldsymbol{K}=\begin{bmatrix}\boldsymbol{K}_r & \boldsymbol{0}\\ \boldsymbol{0} & \boldsymbol{K}_s\end{bmatrix}. \tag{11}$$

The Fig. 1 shows the schematic diagram of different flight forms of the aircraft, namely rolling, pitching and yawing. When the aircraft performs different maneuvering forms, the rotor system will be subjected to different forms of flight loads. When maneuvering load, unbalanced excitation, nonlinear bearing force and oil film force in the rotor system and changes in rotor speed are taken into account, the dynamic equation of the rotor system can be expressed as:

$$\begin{aligned}&\boldsymbol{M}\ddot{\boldsymbol{q}}+\left[\boldsymbol{C}-\omega(t)\boldsymbol{G}+\boldsymbol{C}_B\right]\dot{\boldsymbol{q}}\\ &+\left(\boldsymbol{K}+\boldsymbol{K}_B\right)\boldsymbol{q}=\boldsymbol{F}_e+\boldsymbol{F}_b+\boldsymbol{F}_s+\boldsymbol{F}_B\end{aligned} \tag{12}$$

where $\boldsymbol{M}$, $\boldsymbol{C}$, $\boldsymbol{G}$ and $\boldsymbol{K}$ are the mass, damping, gyroscopic and stiffness matrix of the rotor system respectively. $\boldsymbol{C}_B$ and $\boldsymbol{K}_B$ are the additional damping and stiffness matrix caused by aircraft maneuvering, $\boldsymbol{F}_e$ is the unbalanced force, $\boldsymbol{F}_b$ is the nonlinear bearing force, $\boldsymbol{F}_s$ is the nonlinear oil film force, and $\boldsymbol{F}_B$ is the excitation force caused by aircraft maneuvering.

The speed of the rotor varies linearly with time, the rotation speed of the rotor becomes a function related to time t, and correspondingly, the rotation-related loads, such as maneuvering load, also change with time. Because nonlinear factors such as bearing force and squeeze film forces of the rotor system are taken into account in the model, after the dynamic equation of variable-speed rotor under arbitrary maneuvering flight is established, Newmark-β method and Newton-Raphson method are adopted to solve the response of the rotor system. The modeling and solving process is shown in Fig. 3.

In rotor systems, most structures are multi-degree-of-freedom systems, and Rayleigh damping theory is used to assume that the damping matrix is obtained by superposition of mass and stiffness matrix. This energy dissipation simulation method has great numerical advantages and can meet the needs of general structural dynamic analysis. As the rotor system is a system of multiple degrees of freedom, Rayleigh damping can well estimate the response of the system and adapt to the change of damping ratio under different modes [29]. Therefore, Rayleigh damping theory is used in this paper, which is obtained by the superposition of mass and stiffness matrices. Moreover, this energy dissipation simulation method has great numerical advantages, and many scholars have applied it to the study of rotor dynamics Rayleigh damping form, which can be expressed as [25]:

$$\boldsymbol{C}=\alpha\boldsymbol{M}+\beta\boldsymbol{K} \tag{13}$$

$$\begin{aligned}\alpha&=2\left(\frac{\xi_2}{\omega_2}-\frac{\xi_1}{\omega_1}\right)/\left(\frac{1}{\omega_2^2}-\frac{1}{\omega_1^2}\right)\\ \beta&=2\left(\xi_2\omega_2-\xi_1\omega_1\right)/\left(\omega_2^2-\omega_1^2\right)\end{aligned} \tag{14}$$

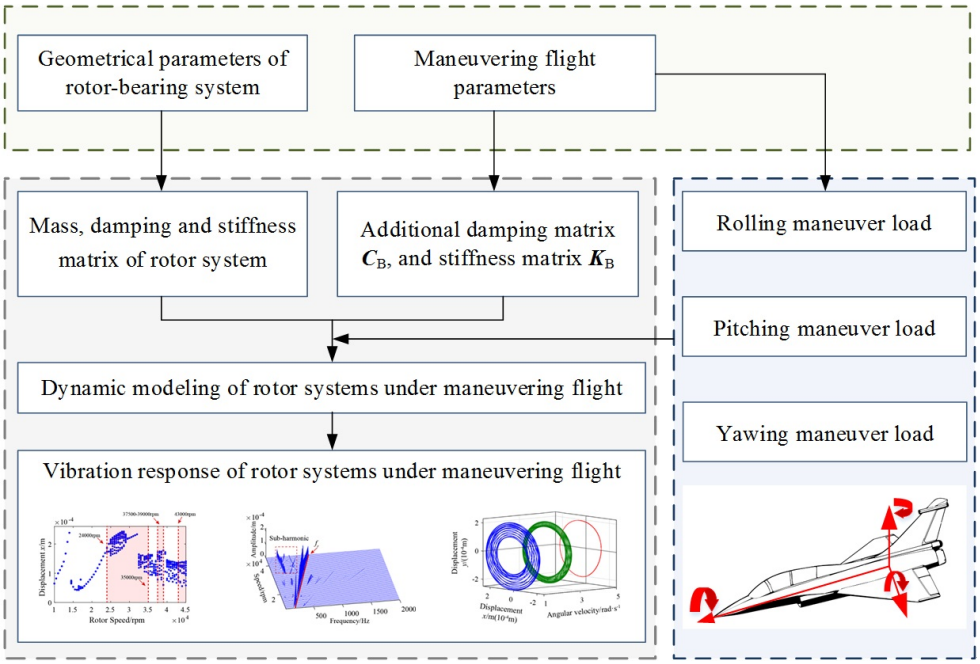

Fig. 3. Flow chart of rotor-bearing system modeling and solution.

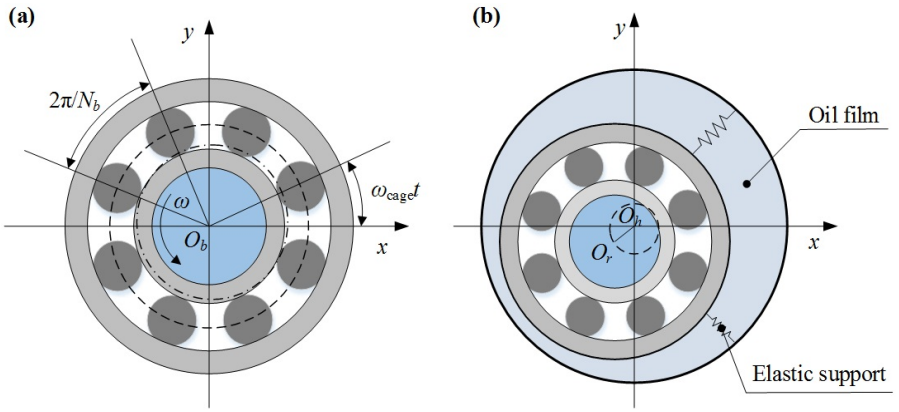

Fig. 4. Schematic diagram of bearing and SFD structure: (a) schematic of rolling bearing; (b) schematic of SFD structure.

where ω_1, ω_2 are the first and second natural angular frequency, ξ_1 and ξ_2 are the first and second modal damping ratios.

In the rotor-bearing system model, rolling bearings with SFD are supported on both sides, as shown in Fig. 4. Both rolling bearings and SFD introduce nonlinear forces to the rotor system. Based on Hertz contact theory, the nonlinear restoring force in ball bearings can be expressed as follows:

$$\begin{aligned} F_{bx} &= \sum_{i=1}^{N_b} C_b \left(x\cos\theta_i + y\sin\theta_i - \gamma_0\right)^{3/2} \\ &\quad \times H\left(x\cos\theta_i + y\sin\theta_i - \gamma_0\right)\cos\theta_i \\ F_{by} &= \sum_{i=1}^{N_b} C_b \left(x\cos\theta_i + y\sin\theta_i - \gamma_0\right)^{3/2} \\ &\quad \times H\left(x\cos\theta_i + y\sin\theta_i - \gamma_0\right)\sin\theta_i \end{aligned} \tag{15}$$

where N_b is the number of rolling elements, C_b is the Hertz contact stiffness, x and y represent the relative displacements between the rotor and outer ring. According to the hypothesis of the short bearing, the nonlinear oil film force in the x and y directions can be expressed as [14]:

$$\begin{cases} F_{oilx} = -\dfrac{\mu R L^3}{C^2\sqrt{X_i^2 + Y_i^2}} \begin{pmatrix} X_i\left(I_1\dot{\varepsilon} + I_2\varepsilon\dot{\phi}\right) \\ -Y_i\left(I_2\dot{\varepsilon} + I_3\varepsilon\dot{\phi}\right) \end{pmatrix} \\ F_{oily} = -\dfrac{\mu R L^3}{C^2\sqrt{X_i^2 + Y_i^2}} \begin{pmatrix} Y_i\left(I_1\dot{\varepsilon} + I_2\varepsilon\dot{\phi}\right) \\ +X_i\left(I_2\dot{\varepsilon} + I_3\varepsilon\dot{\phi}\right) \end{pmatrix} \end{cases}. \tag{16}$$

I_1, I_2, and I_3 are the Sommerfeld integrals, and θ_1 is the starting point of the oil film positive pressure zone

$$\begin{cases} I_1 = \int_{\theta_1}^{\theta_2} \dfrac{\cos^2\theta}{(1+\varepsilon\cos\theta)^3}\mathrm{d}\theta \\ I_2 = \int_{\theta_1}^{\theta_2} \dfrac{\sin\theta\cos\theta}{(1+\varepsilon\cos\theta)^3}\mathrm{d}\theta \\ I_3 = \int_{\theta_1}^{\theta_2} \dfrac{\sin^2\theta}{(1+\varepsilon\cos\theta)^3}\mathrm{d}\theta \\ \theta_1 = \tan^{-1}\left(-\dfrac{\dot{\varepsilon}}{\varepsilon\dot{\phi}}\right). \end{cases} \tag{17}$$

The number of rolling elements on the left bearing is 17, the bearing clearance is 0.02 mm, the inner and outer race diameters are 46 mm and 73.7 mm respectively, the number of rolling elements on the right is 18, and the inner and outer race diameter are 50 mm and 73.4 mm respectively. The center spring stiffness of the left and right SFDs are 1.7e7 N/m and 2.55e7 N/m, respectively, the clearance is 0.2 mm, the oil film diameter is 79.7 mm and 77.5 mm, respectively, and the oil film width is 11 mm.

3. Model validation

The rotor system established in this paper uses rolling bearings as supporting components. In the process of rotation, the rolling bearing stiffness changes periodically due to the periodic movement of the ball, resulting in VC vibration. In this paper, Hertz contact theory is used to establish a mathematical model of rolling bearings, and the calculation results are compared with those in the published literature to verify the correctness of the method used in this paper.

It can be seen from Figs. 5 and 6 that the results obtained in this paper are in good agreement with those in the literature, it can be considered that the method used in this paper to calculate the dynamic characteristics of the rotor with nonlinear forces is correct.

4. Results and discussion

In the following discussion, the effect of speed variation and different maneuvering loads on the dynamic characteristics of the rotor system was analyzed. The rotor system has uniform parameters, the geometric and material parameters of the model are shown in Appendix. Add the unbalance at node 6 (disk 1) as 2e-4 kg·m, and select the node 6 as the response node.

4.1 Influence of the rotating speed

The rotor system slows down with a time scale of about 10^{-1}-10^{1} s [28]. And the vibration characteristics of the rotor system are discussed when the speed changes. Fig. 7 shows the shaft orbit and time domain diagram of disk 1 when the speed drops from 45000 rpm to 3000 rpm. Fig. 7(a) shows that the displacement in horizontal and vertical directions is symmetric. Fig. 7(b) shows the time domain diagram of disk 1 in the horizontal direction, the rotation speed of the rotor system is 45000 rpm at 0-0.5 s, and drops to 3000 rpm at 0.5-1.5 s, and the rotation speed remains at 3000 rpm at 1.5-2 s. The rotor system presents nonlinear vibration characteristics at 45000 rpm, and in the deceleration stage, the rotor experiences two-order critical speeds.

To further explore the influence of the variation of rotation

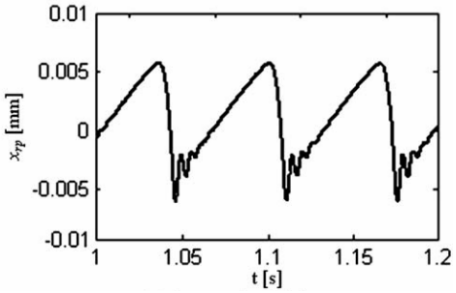

(a) Results in the Ref. [30]

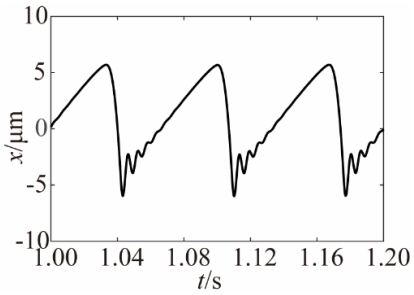

(b) Results in this paper

Fig. 5. Horizontal response of rotor turntable (n_r = 300 rpm).

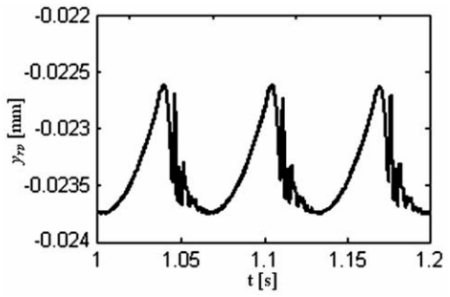

(a) Results in the Ref. [30]

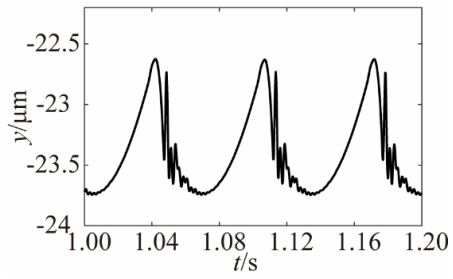

(b) Results in this paper

Fig. 6. Vertical response of rotor turntable (n_r = 300 rpm).

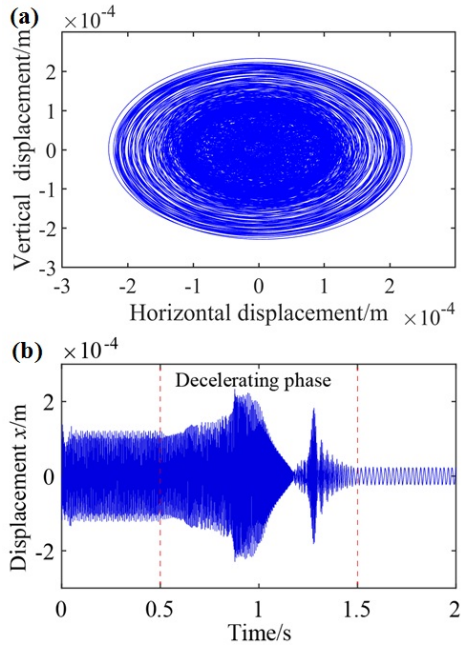

Fig. 7. Response of rotor system with speed variation: (a) shaft orbit diagram; (b) time domain diagram.

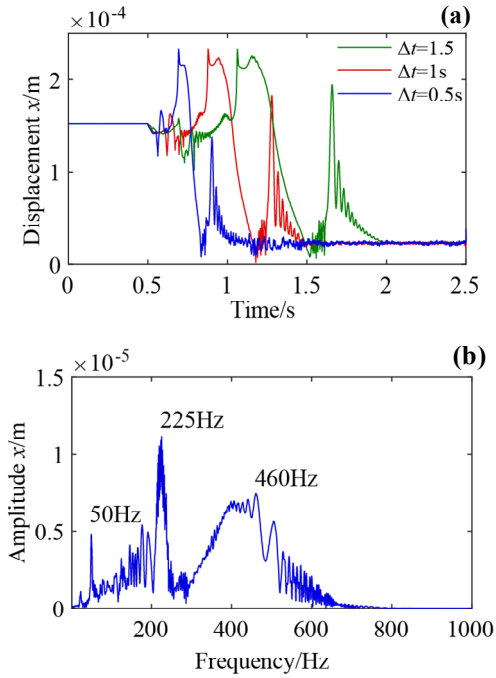

Fig. 8. Rotor system response: (a) envelope diagram; (b) frequency domain diagram.

speed on dynamic characteristics, Fig. 8(a) shows the envelope diagram of time domain response when the rotor drops from 45000 rpm to 3000 rpm in different time periods. The rotation speed starts to decrease at 0.5 s, and the time of deceleration Δt is 0.5 s, 1 s and 1.5 s respectively. It can be seen that the faster the speed decreases, the lower the amplitude of the rotor at the critical speed. Therefore, the rotor speed should

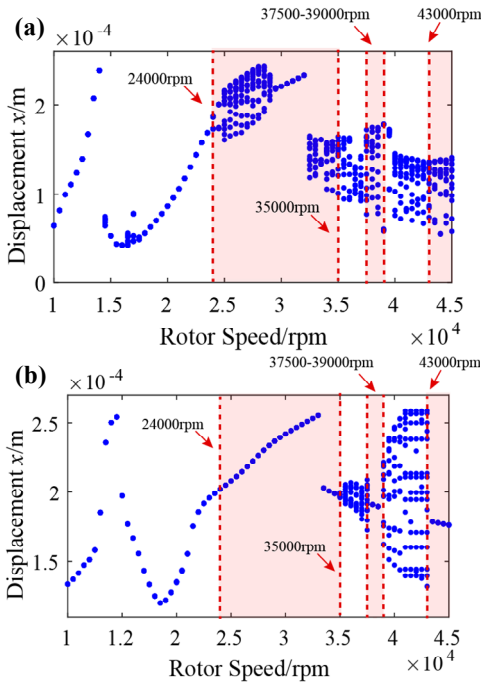

Fig. 9. Bifurcation diagram of rotor system under different rolling maneuvering loads: (a) ω_z = 1 rad/s; (b) ω_z = 5 rad/s.

be minimized in the shortest possible time.

To highlight the characteristics of the rotor system at the deceleration stage, the frequency domain diagram at 0.5 s-2 s and Δt = 1 is shown in Fig. 8(b). In addition to the 50 Hz frequency corresponding to 3000 rpm, the rotor system also has a peak near the frequency corresponding to the critical speed during the speed decline stage.

4.2 Rolling maneuver load

In this paper, three kinds of maneuver flight are considered, namely rolling, yawing, and pitching flight. As shown in Fig. 1, when the aircraft moves around the *z*-axis, it is called the rolling maneuver. In this section, the influence of rolling flight on the dynamic characteristics of variable speed rotors is discussed. Fig. 9 shows the bifurcation diagram when the flight speed v = 50 m/s and the angular velocities ω_z are 1 rad/s and 5 rad/s. The rotation speed ranges from 10000 rpm to 45000 rpm, and the interval of rotation speed is 500 rpm. With the increase of rotational speed, the rotor system presents a variety of motion forms. With the increase of rolling maneuver load, on the one hand, the horizontal displacement slightly increases, this increases the maximum displacement of the rotor system, making it more susceptible to faults such as rubbing. On the other hand, the motion forms of the rotor are also affected by the maneuvering load. The motion forms changes within the speed range of 24000-35000 rpm, 37500-39000 rpm and 43000-45000 rpm, when the angular velocity is 1 rad/s, the rotor motion period in the above speed range has single and quasi period, but when the ω_z reaches 5 rad/s, the motion period in the above speed

range is all single period. Generally speaking, single period motion is typically the most desirable state due to its stability and predictability. In contrast, quasi period motion is relatively unstable, more susceptible to small disturbances, and more likely to cause rotor system vibration and imbalance, making it more difficult to control. As can be seen from the previous theoretical analysis, when the aircraft is in maneuvering flight, it will generate additional stiffness and damping on the rotor, and different forms of maneuvering flight will also correspond to different maneuvering loads. The combined effect of these factors changes the dynamic characteristics of the rotor system, causing changes in the motion state of the rotor system.

The three-dimensional spectrum diagram of the rotor system in the *x* direction under rolling maneuvering load is shown in Fig. 10. When the ω_z is 1 rad/s, it can be seen that the 1 times frequency and multiple sub-harmonic frequency components. And when the ω_z reaches 5 rad/s, some of the sub-harmonic components disappear, which is consistent with the results shown in the bifurcation diagram. It is shown that the increase of rolling load can suppress some sub-harmonic components.

To further analyze the dynamic characteristics of the rotor system, the rotor speed at 20000 rpm, 27000 rpm and 45000 rpm was selected to analyze the vibration characteristics. Fig. 11(a) shows the shaft orbit diagram when ω_z is 1 rad/s, 3 rad/s, and 5 rad/s under 20000 rpm, respectively. The rotor system shows a single period motion and with the increase of ω_z, the displacement in both vertical and horizontal directions increase significantly. It is worth noting that the increase in the horizontal displacement is larger than that in the vertical direction. And although the displacement increases with the increase of the maneuvering load, the motion range does show a decreasing trend. When ω_z = 5, the shaft orbit presents an obvious elliptical shape. In Fig. 11(b), the corresponding spectrum diagram in the *x* direction shows that the 1 time frequency component decreases with the increase of rolling load, which is the same as the result in Fig. 10(a).

When the rotor speed reaches 27000 rpm, Fig. 12(a) shows that the motion form of the rotor system gradually becomes

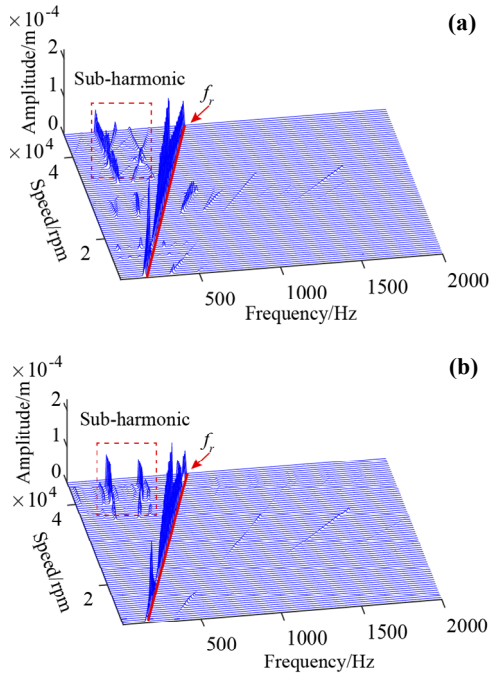

Fig. 10. Three-dimensional spectrogram in x direction under different rolling maneuvering loads: (a) ω_z = 1 rad/s; (b) ω_z = 5 rad/s.

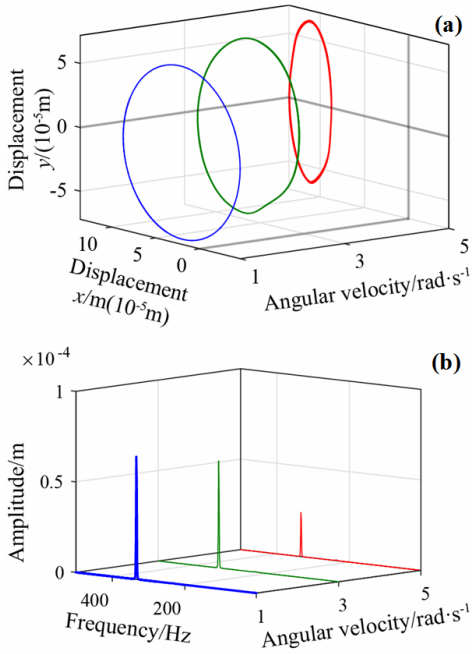

Fig. 11. The shaft orbit and frequency domain diagram under different maneuvering loads (20000 rpm).

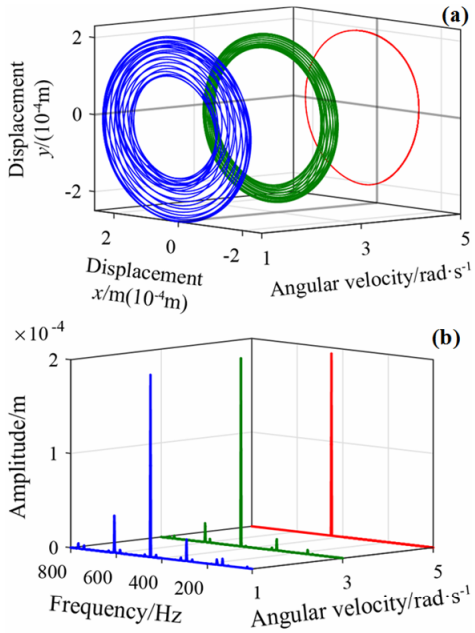

Fig. 12. The shaft orbit and frequency domain diagram under different maneuvering loads (27000 rpm).

single period with the increase of the maneuvering load. In Fig. 12(b), with the increase of the angular velocity, the peak value of the sub-harmonic frequency gradually decreases, but it is worth noting that the 1 time frequency component does not change significantly. Fig. 13 shows the shaft orbit and spectrum diagram in the *x* direction at 45000 rpm. It can be seen from the figure that when the angular velocity increases from 1 rad/s to 3 rad/s, the rotor system has presented a single period,

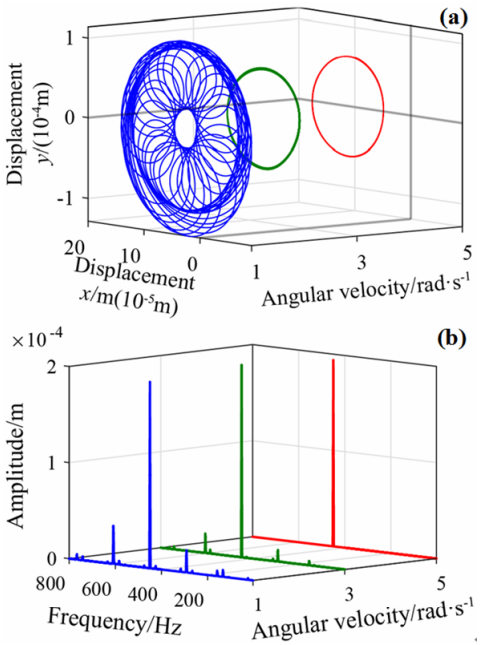

Fig. 13. The shaft orbit and frequency domain diagram under different maneuvering loads (45000 rpm).

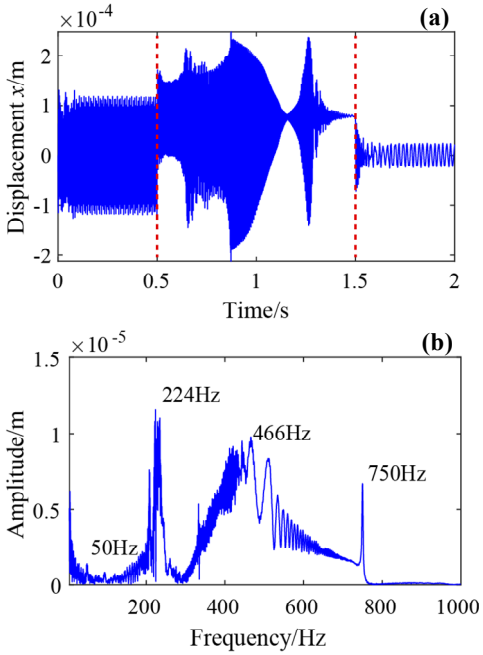

Fig. 14. The time domain and frequency domain diagram (ω_z = 3).

which means that the rotor system is more affected by maneuvering load at the higher speed.

Furthermore, the working state of the rotor system was simulated by considering the influence of speed variation and maneuver load. In Fig. 14, the speed begins to decrease at 0.5 seconds and is simultaneously affected by maneuvering loads. From 0.5 to 1.5 s, the speed decreases from 45000 rpm to 3000 rpm, and after 1.5 seconds, the rotor system's speed stabilizes at 3000 rpm. Due to the influence of maneuvering loads, the displacement of the rotor system is offset during the deceleration phase, and the maximum displacement increases. A sudden change in displacement also occurs near the critical speed. In the frequency spectrum, as shown in Fig. 14(b), in addition to the two stable operating stages corresponding to 50 Hz and 750 Hz in the 0-0.5 s and 1.5-2 s periods, there are many small frequency components due to the time-varying speed of the rotor system. Furthermore, the frequency peak corresponding to the critical speed still exists.

4.3 Pitching maneuver load

This section discusses the effect of pitching maneuver load on the dynamics of the variable speed rotor. The pitching maneuver load is generated when the aircraft moves around the *x*-axis. Fig. 15 shows the bifurcation diagram when the rotor system is subjected to maneuvering loads. The effect of pitching maneuver load on the rotor system is similar to that of rolling maneuver load. The horizontal displacement will be slightly increased, and the motion form will be affected. When the ω_x is

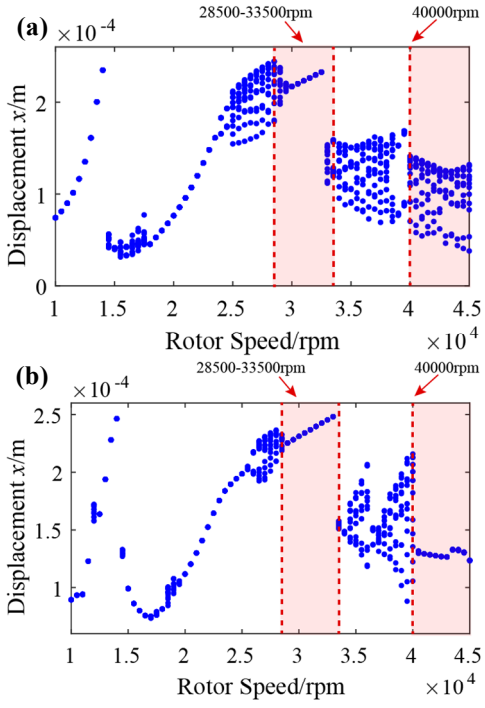

Fig. 15. Bifurcation diagram of rotor system under different pitching maneuvering loads: (a) ω_x = 1 rad/s; (b) ω_x = 5 rad/s.

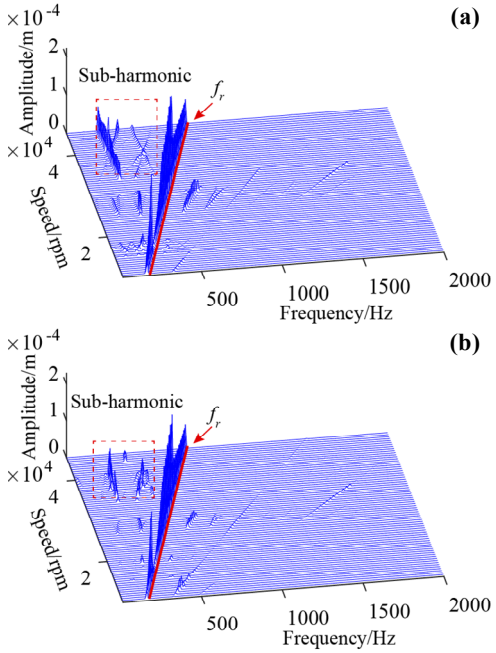

Fig. 16. Three-dimensional spectrogram in *x* direction under different pitching maneuvering loads: (a) ω_z = 1 rad/s; (b) ω_z = 5 rad/s.

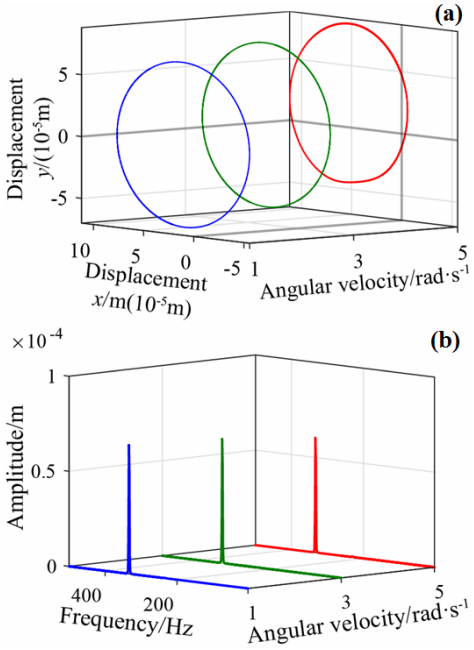

Fig. 17. The shaft orbit and frequency domain diagram under different maneuvering loads (20000 rpm).

1rad/s, the motion period is the single and quasi-periodic period between 28500-33500 rpm and 40000-45000 rpm. However, when the ω_x increases to 5 rad/s, the motion period in the above speed range becomes single period.

Fig. 16 shows the three-dimensional spectrum diagram of the rotor system under different maneuvering loads. With the increase of ω_x, some sub-harmonic components disappear, which is like the impact of rolling load. And it can be found that the impact of pitching maneuver load on the harmonic components is smaller than that of rolling load.

In order to discuss the effect of pitching maneuver load on the vibration characteristics, the rotor at speeds of 20000 rpm, 27000 rpm and 45000 rpm were selected for analysis. As shown in Fig. 17(a), when the rotor system is affected by pitching maneuver load, the displacement of the rotor in both horizontal and vertical tends to increase, but less than that of the rolling maneuver load, and the range of motion changes less. Its amplitude also shows a decreasing trend, but compared with the rolling maneuver load, its decreasing degree is smaller.

When the speed is 27000 rpm, as shown in Fig. 18(a), with the increase of the pitching maneuver load, the shaft orbit changes little, and motion period does not change. It also can be seen from the spectrum diagram in Fig. 18(b) that the 1 time frequency component of the rotor system does not change significantly with the increase of pitching maneuver load, and the change of sub-harmonic component is also very small compared with the impact of rolling maneuvering load.

Fig. 19 shows the shaft orbit and spectrum diagram in the *x* direction under different maneuvering loads at 45000 rpm. When the ω_x increases from 1 rad/s to 5 rad/s, the motion range of the rotor system gradually decreases, and when the

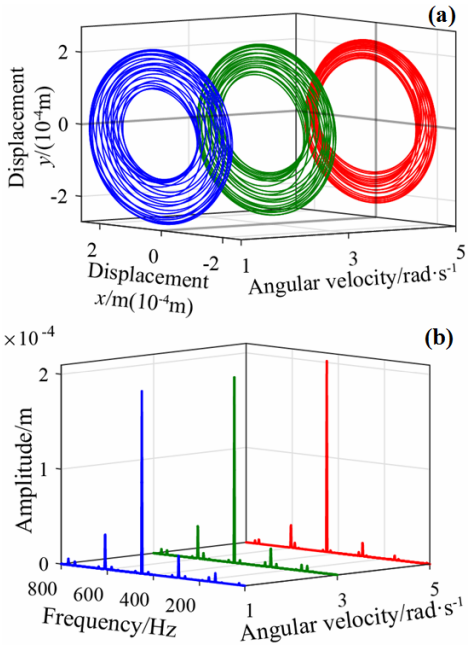

Fig. 18. The shaft orbit and frequency domain diagram under different maneuvering loads (27000 rpm).

angular velocity is 5rad/s, the rotor system moves in a single period. Furthermore, the rotor speed decrease and the influence of pitching maneuver load are considered. In Fig. 20(a), the rotor system's speed decreases from 45000 rpm to 3000 rpm in the range of 0.5-1.5, and is subjected to pitch maneuvering loads. It can be observed that the displacement of the rotor system is translated due to the influence of maneuver-

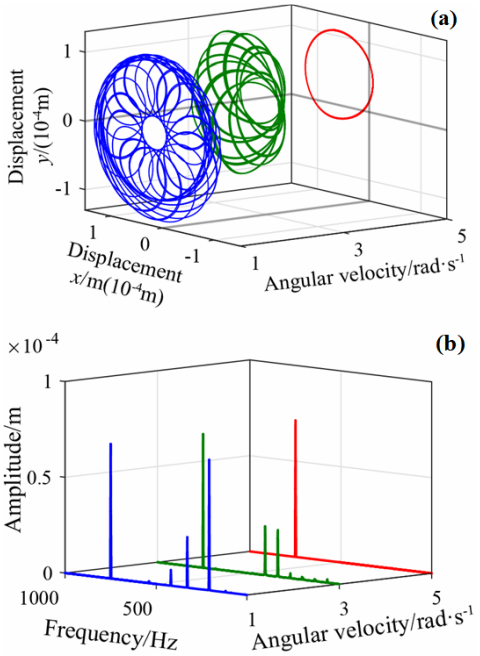

Fig. 19. The shaft orbit and frequency domain diagram under different maneuvering loads (45000 rpm).

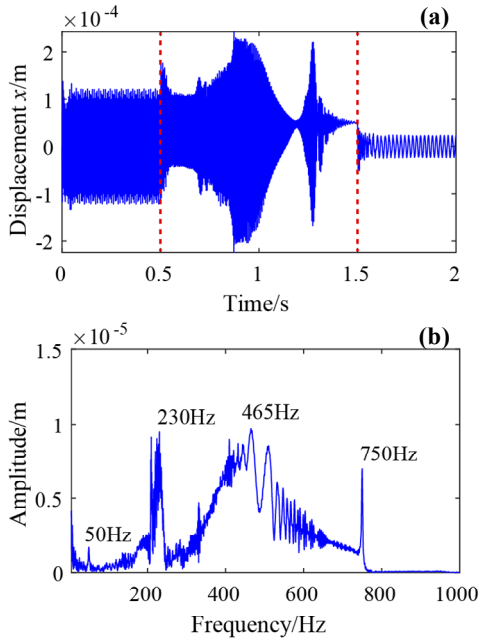

Fig. 20. The time domain and frequency domain diagram (ω_x = 3).

ing loads, but to a lesser extent than the effect of rolling maneuver load. The response also exhibits a peak near the critical speed, which is also reflected in the frequency components shown in Fig. 20(b).

4.4 Yawing maneuver load

The influence of yawing maneuver load on the dynamics of variable speed rotors is discussed in this section. Yawing maneuvering load will occur when the aircraft moves around the *y*-axis. Fig. 21 is the bifurcation diagram under different yawing maneuver loads. As a whole, the yawing maneuvering load can reduce the horizontal displacement, which is opposite to the effect of rolling and pitching maneuvering loads. It also has a certain influence on the motion forms, the yawing maneuvering load changes the motion period of the rotor system within the speed range of 29000-35000 rpm and 40500-45000 rpm. It can also be seen from Fig. 22 that when the yaw load increases, the sub-harmonic component decreases.

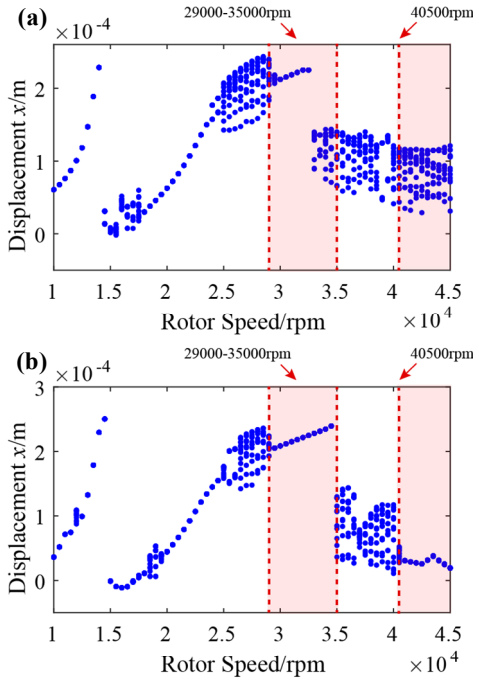

Fig. 21. Bifurcation diagram of rotor system under different rolling maneuvering loads: (a) ω_y = 1 rad/s; (b) ω_y = 5 rad/s.

Furthermore, the rotor system at speeds of 20000 rpm, 27000 rpm and 45000 rpm was selected as the analysis objects to analyze the influence of yawing maneuver load on the dynamic characteristics. In Fig. 23(a), with the increase of maneuvering load, the displacement in the *y* direction still shows an increasing trend, but the displacement in the *x* direction shows a decreasing trend, and the range of motion of the rotor system hardly changes, which can be mutually verified with the results in Fig. 23(b). When the rotation speed is 27000 rpm, the maneuvering load still has a certain degree of influence on the motion form, but compared with the rolling and pitching maneuver load, the influence degree is smaller. Fig. 24 shows that the increase of yawing maneuvering load has little influence on the rotor system, the 1 times frequency and multiple sub-harmonic frequency components have almost no change. Fig. 25 shows the shaft orbit and spectrum diagram at 45000 rpm. When the ω_y increases from 1 to 3 rad/s, the displacement and motion period change, and when the ω_y increases to 5, the rotor system shows in a single period.

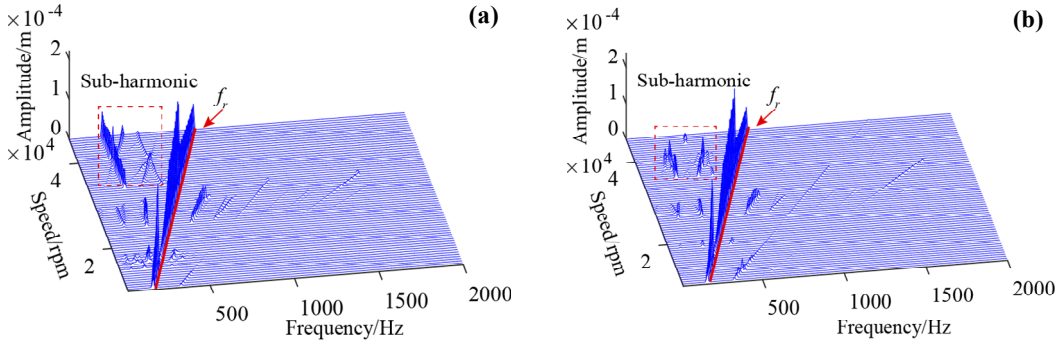

Fig. 22. Three-dimensional spectrogram in *x* direction under different pitching maneuvering loads: (a) ω_y = 1 rad/s; (b) ω_y = 5 rad/s.

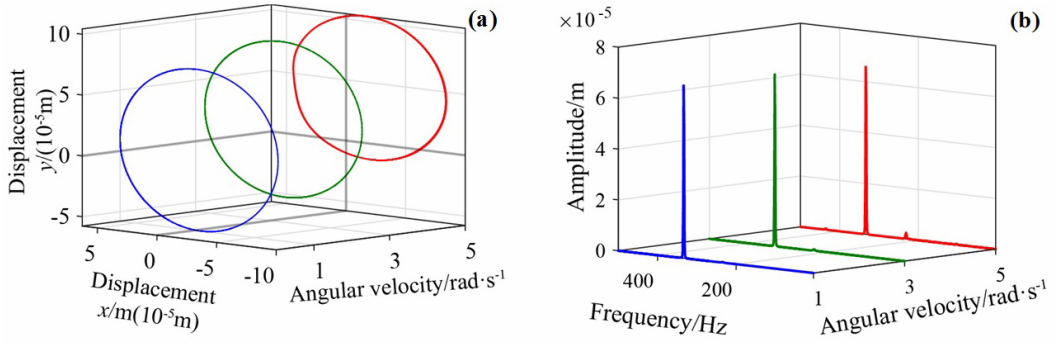

Fig. 23. The shaft orbit and frequency domain diagram under different maneuvering loads (20000 rpm).

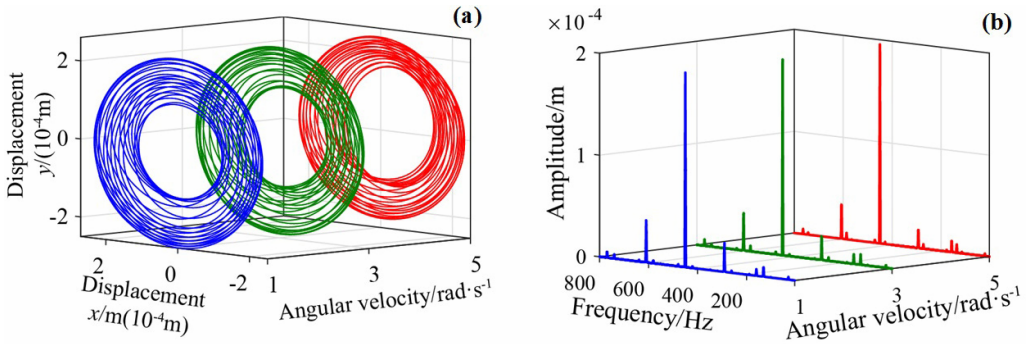

Fig. 24. The shaft orbit and frequency domain diagram under different maneuvering loads (27000 rpm).

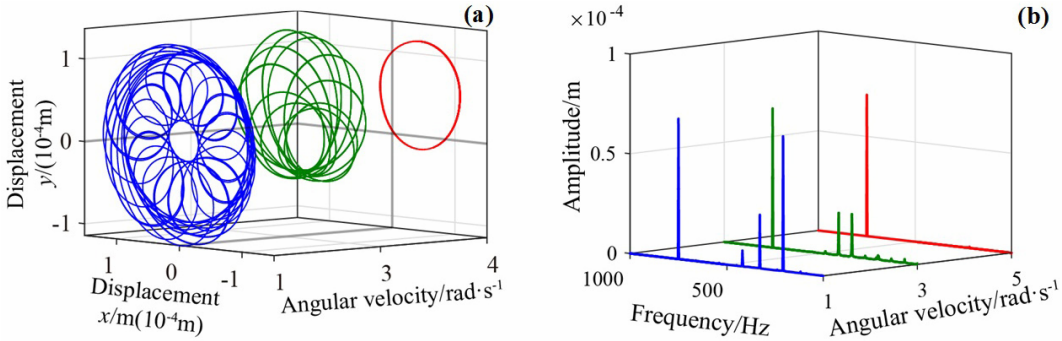

Fig. 25. The shaft orbit and frequency domain diagram under different maneuvering loads (45000 rpm).

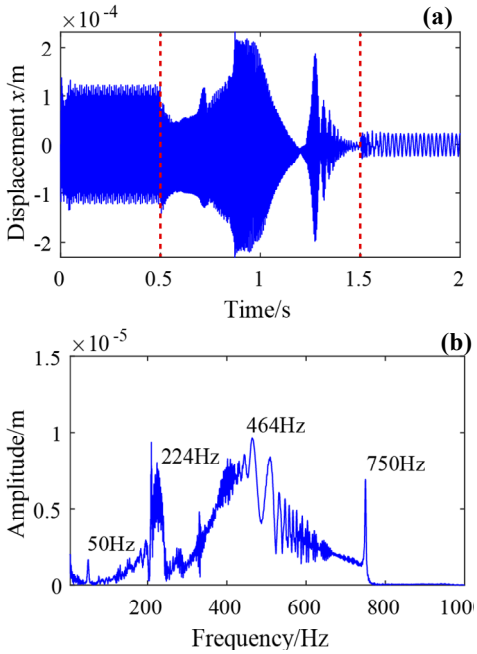

Fig. 26. The time domain and frequency domain diagram (ω_y = 3).

The effect of yawing maneuver load on the rotor system is considered. It can be seen from Fig. 26 that yaw maneuvering loads also offset the displacement of the rotor system. But its direction is opposite to the other two loads, and the degree of displacement change is small, which means that yaw maneuvering load is less likely to cause the failure of the rotor system.

5. Conclusions

In this paper, a rotor dynamic model which can consider arbitrary maneuvering flight and rotor speed variation is established. Furthermore, the bearing and SFD structure are also considered in the model. Finally, the influence of rotation speed variation, rolling, pitching and yawing maneuver loads on the dynamic characteristics are analyzed, and the following conclusions are drawn:

1) When the rotor passes the critical speed during deceleration, the response amplitude changes quickly, and the deceleration time has a great influence on the transient peak. With the shortening of deceleration time, the vibration response of the rotor decreases at the critical speed. Therefore, it is safer for the rotor system to complete the variation of speed in a shorter time.

2) The maneuvering load will affect the motion period of the rotor system, and the higher the speed, the more obvious the influence. In the model established in this paper, the motion period of the rotor is more easily changed from quasi-period to single period by maneuvering load at a higher speed.

3) According to the established model in this paper, when the rotor system moves in a single period, the 1 times frequency components will be affected by the maneuvering load, when the rotor system presents quasi-periodic motion, the maneuvering load mainly inhibits the sub-harmonic component, but has little effect on the 1 times frequency components.

4) Rolling maneuver load has the greatest influence on the displacement of the rotor system. The influence of pitching maneuver load is like that of rolling flight, but to a lesser extent, the effects of yaw maneuvering loads are opposite to those of rolling and pitching loads, and have the least influence.

Acknowledgments

The research work is supported by the National Science and Technology Major Project (2017-I-0006-0007), the National Natural Science Foundation of China (52005100), the National Science Foundation for Distinguished Young Scholars (52125209), the Key R&D Plan of Jiangsu Province (BE2022158), the Jiangsu Association for Science and Technology Young Talents Lifting Project (TJ-2022-043), the Zhishan Youth Scholar Program of SEU (2242021R41169) and the Fundamental Research Funds for the Central Universities.

Nomenclature

T_t : Translational kinetic energy
T_r : Rotational kinetic energy
$\boldsymbol{v}_B$: Velocity of the aircraft
$\bar{\boldsymbol{\omega}}_B$: Angular velocity of the aircraft
ω : Rotor speed
φ_0 : Initial angle of disk unbalance
$\dot{X}_B$, $\dot{Y}_B$, $\dot{Z}_B$: Aircraft velocity along coordinate axis
ω_x, ω_y, ω_z: Angular velocity around coordinate axis.
J_d : Diameter moment of inertia of the disk
J_p : Polar moment of inertia of the disk
$\boldsymbol{C}_B$: Additional damping matrix
$\boldsymbol{K}_B$: Additional stiffness matrix
$\boldsymbol{F}_B$: Maneuvering load
m_{sl}, m_{sr} : Concentrated mass SFD
k_{blx}, k_{bly} : Stiffness of the elastic support on the left
k_{brx}, k_{bry} : Stiffness of the elastic support on the right
$\boldsymbol{M}$: Mass matrix of the rotor system
$\boldsymbol{C}$: Damping matrix of the rotor system
$\boldsymbol{G}$: Gyroscopic matrix of the rotor system
$\boldsymbol{K}$: Stiffness matrix of the rotor system
$\boldsymbol{F}_e$: Unbalanced force
$\boldsymbol{F}_b$: Nonlinear bearing force
$\boldsymbol{F}_s$: Nonlinear oil film force
ω_1, ω_2 : First and second natural angular frequency
ξ_1, ξ_2 : First and second modal damping ratios
Δt : Time of deceleration

References

[1] J. Y. Xie, N. X. Guan, M. Zhou and Z. F. Xie, Study on the mechanism of the variable-speed rotor affecting rotor aerodynamic performance, *Applied Sciences*, 8 (2018) 1030.
[2] Z. Y. Lu, S. Zhong, H. Z. Chen, X. D. Wang, J. J. Han and C.

Wang, Nonlinear response analysis for a dual-rotor system supported by ball bearing, *International Journal of Non-Linear Mechanics*, 128 (2021) 103627.

[3] S. Amirzadegan, M. Rokn-Abadi and R. D. Firouz-Abadi, Optimization of nonlinear unbalanced flexible rotating shaft passing through critical speeds, *International Journal of Structural Stability and Dynamics*, 22 (1) (2021) 2250014.

[4] J. Liu, C. K. Tang and G. Pan, Dynamic modeling and simulation of a flexible-rotor ball bearing system, *Journal of Vibration and Control*., 28 (23-24) (2021) 3495-3509.

[5] Y. Q. Li, Z. Luo, Z. J. Liu and X. J. Hou, Nonlinear dynamic behaviors of a bolted joint rotor system supported by ball bearings, *Archive of Applied Mechanics*, 89 (2019) 2381-2395.

[6] J. Z. Liu, Q. G. Fei, S. Q. Wu, Z. H. Tang, S. F. Liao and D. H. Zhang, An efficient dynamic modeling technique for a central tie rod rotor, *International Journal of Aerospace Engineering*, 2021 (2021) 6618828.

[7] Y. Wei, Z. B. Chen and E. H. Dowell, Nonlinear characteristics analysis of a rotor-bearing-brush seal system, *International Journal of Structural Stability and Dynamics*, 18 (5) (2018) 1850063.

[8] G. F. Nan, Y. Zhang, Y. J. Zhu and W. Guo, Nonlinear dynamics of rotor system supported by bearing with waviness, *Science Progress*, 103 (3) (2020) 1-29.

[9] Y. L. Jin, K. Lu, C. X. Huang, L. Hou and Y. S. Chen, Nonlinear dynamic analysis of a complex dual rotor-bearing system based on a novel model reduction method, *Applied Mathematical Modelling*, 75 (2019) 553-571.

[10] Y. F. Wang, Y. H. Ma and J. Hong, Study on dynamic stiffness of supporting structure and its influence on vibration of rotors, *Chinese Journal of Aeronautics*, 35 (11) (2022) 252-263.

[11] K. Lu, Y. L. Jin, P. F. Huang, F. Zhang, H. P. Zhang, C. Fu and Y. S. Chen, The applications of POD method in dual rotor-bearing systems with coupling misalignment, *Mechanical Systems and Signal Processing*, 150 (2021) 107236.

[12] C. D. Zhou, Y. B. Liu, W. Teng, H. S. Zhang, H. T. He and C. Zhou, Dynamic modeling and stability analysis of a heavy-duty flywheel rotor-bearing system with two cracks, *International Journal of Structural Stability and Dynamics*, 22 (9) (2022) 2250103.

[13] H. B. Wang, Y. L. Zhao, Z. Luo and Q. K. Han, Analysis on influences of squeeze film damper on vibrations of rotor system in aeroengine, *Applied Sciences*, 12 (2) (2022) 615.

[14] X. X. Ma, H. Ma, H. Q. Qin, X. M. Guo, C. G. Zhao and M. Y. Yu, Nonlinear vibration response characteristics of a dual-rotor-bearing system with squeeze film damper, *Chinese Journal of Aeronautics*, 34 (2021) 128-147.

[15] H. F. Wang, A modeling method for a rotor system with an active floating ring squeeze film damper, *Proceedings of the Institution of Mechanical Engineers, Part C: Journal of Mechanical Engineering Science*, 235 (2020) 627-638.

[16] J. Z. Liu, Q. G. Fei, S. Q. Wu, Z. H. Tang and D. H. Zhang, Nonlinear vibration response of a complex aeroengine under the rubbing fault, *Nonlinear Dynamics*, 106 (2021) 1869-1890.

[17] J. Q. Han, G. H. Luo, W. Chen, F. Wang, L. L. Liu, Z. H. Zhao and G. Luo, Coupling vibration analysis of turbine shared support rotorbearing system with squeeze film dampers, *International Journal of Aerospace Engineering*, 131 (2022) 8425735.

[18] K. Ri, K. Kim, C. Yun, K. Kim and T. Choe, Nonlinear vibration and stability analysis of flexible rotor supported on SFD by IHB method, *International Journal of Structural Stability and Dynamics*, 22 (2022) 2250187.

[19] L. Hou, Y. S. Chen, Y. Q. Fu and Z. G. Li, Nonlinear response and bifurcation analysis of a duffing type rotor model under sine maneuver load, *International Journal of Non-Linear Mechanics*, 78 (2016) 133-141.

[20] L. Hou and Y. S. Chen, Bifurcation analysis of aero-engine's rotor system under constant maneuver load, *Applied Mathematics and Mechanics (English Edition)*, 36 (11) (2015) 1417-1426.

[21] L. Hou, Y. S. Chen, Q. J. Cao and Z. Y. Zhang, Turning maneuver caused response in an aircraft rotor-ball bearing system, *Nonlinear Dynamics*, 79 (2015) 229-240.

[22] L. Hou, Y. S. Chen, Q. J. Cao and Z. Y. Lu, Nonlinear vibration analysis of a cracked rotor-ball bearing system during flight maneuvers, *Mechanism and Machine Theory*, 105 (2016) 515-528.

[23] B. B. Han and Q. Ding, Forced responses analysis of a rotor system with squeeze film damper during flight maneuvers using finite element method, *Mechanism and Machine Theory*, 122 (2018) 233-251.

[24] T. Gao, S. Q. Cao and Y. T. Sun, Nonlinear dynamic behavior of a flexible asymmetric aero-engine rotor system in maneuvering flight, *Chinese Journal of Aeronautics*, 33 (10) (2020) 2633-2648.

[25] W. J. Pan, L. Y. Ling, H. Y. Qu and M. H. Wang, Coupling dynamic behavior of aero-engine rotor system caused by rolling, pitching and yawing maneuver loads, *Applied Mathematical Modelling*, 102 (2022) 726-747.

[26] N. Zheng, M. L. Chen, G. H. Luo and Z. F. Ye, Dynamic behavior analysis of intermediate bearing-squeeze film dampers-rotor system under constant maneuvering overload, *Shock and Vibration*, 2021 (2021) 5512409.

[27] W. J. Pan, L. Y. Ling, H. Y. Qu and M. H. Wang, Nonlinear response analysis of aero-engine rotor bearing rub-impact system caused by horizontal yawing maneuver load, *International Journal of Non-Linear Mechanics*, 137 (2021) 103800.

[28] P. C. Yu, D. Y. Zhang, Y. H. Ma and J. Hong, Dynamic modeling and vibration characteristics analysis of the aero-engine dual-rotor system with fan blade out, *Mechanical Systems and Signal Processing*, 106 (2018) 158-175.

[29] Joseph Shibu K., K. Shankar, C. K. Babu and G. K. Degaonkar, Multi-objective optimisation of a small aircraft turbine engine rotor system with self-updating rayleigh damping model and frequency-dependent bearing-pedestal model, *Proceedings of the Institution of Mechanical Engineers, Part C: Journal of Mechanical Engineering Science*, 233 (16) (2019) 5710-5723.

[30] G. Chen, Study on nonlinear dynamic response of an unbalanced rotor supported on ball bearing, *Journal of Vibration and Acoustics*, 131 (6) (2009) 061001.

Appendix

Table A.1. Geometric parameters of finite element model of wheel disc structure (mm).

	L	R_{in}	R_{out}
Sec_1	34.65	34.5	42.57
Sec_2	10.89	34.5	45.54
Sec_3	19.31	34.5	45.54
Sec_4	26.24	34.5	50.49
Sec_5	18.22	52	59.4
Sec_6	22.87	60	66.33
Sec_7	30.69	77	83.16
Sec_8	22.87	60	66.33
Sec_9	25.74	100	109.9
Sec_{10}	23.27	100	107.9
Sec_{11}	36.14	92	99.99
Sec_{12}	43.07	93	111.9
Sec_{13}	25.74	42.5	133.3
Sec_{14}	17.62	42.5	90.09
Sec_{15}	36.53	74	90.09
Sec_{16}	36.63	85	92.07
Sec_{17}	19.8	42.4	75.44
Sec_{18}	19.8	42.4	79.2
Sec_{19}	34.65	42.4	54.45
Sec_{20}	16.83	34.5	49.5
Sec_{21}	21.38	34.5	49.5

Table A.2. Geometric parameters of finite element model of center tie rod structure (mm).

	L	R_{in}	R_{out}
Sec_1	18.22	36.9	40
Sec_2	22.87	36.9	40
Sec_3	43.07	36.9	40
Sec_4	25.74	36.9	40
Sec_5	23.27	36.9	40
Sec_6	36.14	36.9	40
Sec_7	43.07	36.9	40
Sec_8	25.74	36.9	40
Sec_9	17.62	34.5	42.5
Sec_{10}	4.95	34.5	68
Sec_{11}	40.29	34.5	52
Sec_{12}	28.12	34.5	37.7
Sec_{13}	19.8	34.5	37.7
Sec_{14}	19.8	34.5	37.7
Sec_{15}	34.65	34.5	38

Zhang Dahai is an Associate Professor of the School of Mechanical Engineering, Southeast University, Nanjing, China. He received his Ph.D. in School of Mechanical Engineering from Southeast University. His research interests include aero-engine rotor system dynamics, and mechanical behavior of lightweight porous materials and their composite structures.

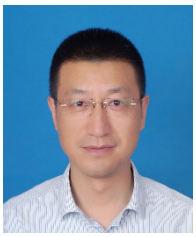

Fei Qingguo is a Full Professor of the School of Mechanical Engineering, Southeast University, Nanjing, China. He received his Ph.D. in Nanjing University of Aeronautics and Astronautics. His research interests include Aerospace mechanical dynamics.